

A convenient ultrasonic path for van der Waals heterostructure construction: Study on MoS_2/graphene as an example

Wen Zhang(张文), Mingyang Gao(高铭阳), Jun Guo(郭俊), Licun Fu(付立存), Ling Liu(刘玲), Jing Wang(王京), and Teng Ma(马腾)

Citation: Chin. Phys. B, 2025, 34 (**11**): 117304. DOI: 10.1088/1674-1056/ade4ae
http://cpb.iphy.ac.cn; http://iopscience.iop.org/cpb

What follows is a list of articles you may be interested in

Ultrafast electron transport in 2D van der Waals heterostructures Bi_2Te_3/Fe_4GeTe_2 probed by terahertz spectroscopy

Hui-Xiang Hong(洪晖祥), Yun Sun(孙芸), Jing Li(李竞), Jing-Yi Peng(彭静宜), Hui-Ping Zhang(张慧萍), Hong-Guang Li(李宏光), Shao-Hui Wu(吴少晖), Tian-Xiao Nie(聂天晓), Yan Peng(彭滟), and Zuan-Ming Jin(金钻明)

Chin. Phys. B, 2025, 34 (**7**): 077304. DOI: 10.1088/1674-1056/adcdf2

Modulating electronic properties of carbon nanotube via constructing one-dimensional vdW heterostructures

Wenqi Lv(吕雯祺), Weili Li(李伟立), Wei Ji(季威), and Yanning Zhang(张妍宁)

Chin. Phys. B, 2025, 34 (**6**): 067303. DOI: 10.1088/1674-1056/adc406

Intrinsic valley-polarized quantum anomalous Hall effect in a two-dimensional germanene/MnI_2 van der Waals heterostructure

Xiao-Jing Dong(董晓晶) and Chang-Wen Zhang(张昌文)

Chin. Phys. B, 2024, 33 (**7**): 077303. DOI: 10.1088/1674-1056/ad4bbd

Field induced Chern insulating states in twisted monolayer-bilayer graphene

Zhengwen Wang(王政文), Yingzhuo Han(韩英卓), Kenji Watanabe, Takashi Taniguchi, Yuhang Jiang(姜宇航), and Jinhai Mao(毛金海)

Chin. Phys. B, 2024, 33 (**6**): 067301. DOI: 10.1088/1674-1056/ad3b8a

Improving the electrical performances of InSe transistors by interface engineering

Tianjun Cao(曹天俊), Song Hao(郝松), Chenchen Wu(吴晨晨), Chen Pan(潘晨), Yudi Dai(戴玉頔), Bin Cheng(程斌), Shi-Jun Liang(梁世军), and Feng Miao(缪峰)

Chin. Phys. B, 2024, 33 (**4**): 047302. DOI: 10.1088/1674-1056/ad24d7

A convenient ultrasonic path for van der Waals heterostructure construction: Study on MoS_2/graphene as an example

Wen Zhang(张文)[1,†], Mingyang Gao(高铭阳)[2,4,†,‡], Jun Guo(郭俊)[1], Licun Fu(付立存)[3], Ling Liu(刘玲)[1], Jing Wang(王京)[1], and Teng Ma(马腾)[1]

[1] *Mechanical and Electrical Engineering Department, Inner Mongolia Technical College of Mechanics & Electrics, Hohhot* 015501, *China*
[2] *School of Electronic Information, Northwest University, Xi'an* 710127, *China*
[3] *School of Physics and Optoelectronic Engineering, Anhui University, Hefei* 230601, *China*
[4] *School of Materials Science and Engineering, Nanyang Technological University, Singapore* 639798, *Singapore*

(Received 23 March 2025; revised manuscript received 4 May 2025; accepted manuscript online 16 June 2025)

Ultrasound is a powerful tool in materials processing, yet its application in constructing van der Waals (vdW) heterostructures remains under-explored. In this study, MoS_2 and graphene — two widely studied 2D materials — were successfully assembled into vdW heterostructures via a convenient ultrasound-driven self-assembly approach. The morphology of the heterostructures was characterized by scanning electron microscopy (SEM), while their structural and compositional features were confirmed through x-ray diffraction (XRD), Raman spectroscopy, and x-ray photoelectron spectroscopy (XPS). Red-shifted Raman peaks and decreased binding energies in XPS spectra provided strong evidence of successful heterostructure formation. A three-stage assembly mechanism — comprising dispersion, assembly, and adjustment — is proposed, with acoustic cavitation playing a key role in driving the process. This study not only demonstrates the feasibility of synthesizing 2D heterostructures via an ultrasonic route but also lays a foundation for future scalable, energy-efficient fabrication strategies.

Keywords: van der Waals heterostructure, ultrasound assembly, MoS_2, graphene

PACS: 73.63.Rt, 43.35.+d, 81.07.–b, 81.16.Dn

DOI: 10.1088/1674-1056/ade4ae **CSTR:** 32038.14.CPB.ade4ae

1. Introduction

Since the discovery of graphene, a growing number of layered 2D materials have been explored and synthesized because of their unique electronic properties and structures. 2D heterostructure enables the investigation of various intriguing physical phenomena in layered 2D materials, and opens up vast potential for practical applications by assembling different 2D layered materials.[1] In contrast to bulk materials with limited interfaces, vdW heterostructure fully leverages the unique electronic properties of the interface region, which spans from a few to tens of nanometers.[2,3] The generation, restriction, and transport of excitons, phonons, photons and carriers in the atomic-level interface can be effectively controlled through the vdW heterostructures.[4–7]

Unlike 3D materials, where the lattice structure is periodically arranged and connected by chemical bonds, in 2D layered materials, one dimension is compressed to the atomic scale, and the layers are held together by weak vdW forces rather than chemical bonds.[8] Previous research has suggested that ultrasound with sufficient power can disrupt the weak vdW forces between layers of 2D materials, making it a viable method for synthesizing few-layer 2D materials.[9–11] Furthermore, the assembly of heterostructures via liquid-phase ultrasound has also been proven to be feasible.[12,13] Currently, there are four other common methods for synthesizing vdW heterostructures: high-temperature solid-state reaction, chemical vapor deposition (CVD), wet-chemical method and mechanical exfoliation.[3,14–16] In contrast, the liquid-phase ultrasound assembly method offers the advantages of exceptional simplicity and energy efficiency. A simple comparison of the methods is provided in Table 1. It is clear from the table that, both in terms of the equipment required for synthesizing the materials and the atmospheric and temperature conditions needed, the ultrasonic assembly method has lower requirements.

Molybdenum disulfide (MoS_2) is a representative 2D layered material comprising Mo layers sandwiched between two S layers.[17] Due to its direct narrow band gap, excellent electrical, chemical and mechanical properties, MoS_2 is considered highly promising for applications in power nanodevices, photonics, energy storage and flexible electronics.[18–20] Graphene, a 2D material renowned for its high electron mobility, comprises carbon atoms arranged in a hexagonal honeycomb lattice formed by sp^2-hybridized orbitals, and can be used as an attractive support layer.[21] Due to the relatively low charge separation rate and conductivity of MoS_2, it is of-

†These authors have contributed equally to this study.
‡Corresponding author. E-mail: mingyanggao6@163.com

© 2025 Chinese Physical Society and IOP Publishing Ltd. All rights, including for text and data mining, AI training, and similar technologies, are reserved.

ten combined with graphene to form a composite structure for enhanced performance.[18,22–24] The MoS_2/graphene heterostructure finds wide applications in electronics, photocatalysis, photonics, etc.[25–27]

Table 1. Comparison of common methods for synthesizing vdW heterostructures in terms of the required instruments, atmosphere and temperature.

Method	Required instruments	Required atmosphere	Required temperature
High-temperature solid-phase reaction method	Tube furnace or muffle furnace, and associated equipment	Rare gas/vacuum/nitrogen/ordinary atmospheric environment	High temperature
Chemical vapor deposition method	Tube furnace and associated equipment	Rare gas/nitrogen/reactive gas environment	High temperature
Wet-chemical method	Ultrasonic machine, high-temperature furnace, reaction kettle, etc	Normal/vacuum/rare gas/nitrogen environment	High temperature
Mechanical exfoliation	2D material transfer stage and associated equipment	Vacuum/normal environment	Room temperature
Ultrasound assembly method	Normal ultrasonic machine	Normal environment	Room temperature

In this study, 2D layered MoS_2 and graphene dispersions are first prepared using ultrasonic water bath exfoliation. Next, an ultrasonic assembly method synthesizes MoS_2/graphene vdW heterostructures with varying mass ratios. SEM, XRD and Raman spectroscopy were used to characterize the synthesized materials. The characterization results confirmed the successful synthesis of the heterostructures and validated the feasibility of the ultrasonic assembly method.

2. Experiment details

2.1. Materials

Analytical-grade MoS_2 powder and graphene powder were used directly without further purification. Bulk MoS_2 powder was purchased from Shanghai Aladdin Biochemical Technology Co. Ltd (Shanghai, China), with a crystallinity of 99.995% and approximate crystal dimensions of 0.5 cm×0.5 cm×0.1–0.15 mm. Layered graphene powder was obtained from Hengqiu Tech. Inc. (Suzhou, China), featuring flake diameters in the range of several tens of micrometers and a specific surface area of 600–1000 m^2/g. Ultrasonic exfoliation was performed to obtain few-layer graphene. Analytical grade Rhodamine B (RhB) dye was purchased from Shanghai Aladdin Technology Co. Ltd (Shanghai, China). All absolute ethanol (analytical grade, AEA) used in the experiments was purchased from Tianjin Kermel Chemical Reagent Co. Ltd (Tianjin, China).

2.2. Preparation of MoS_2 and graphene nanosheets

Similar to previous studies, both graphene nanosheets and 2D sheet-like MoS_2 were prepared via ultrasonic exfoliation using a water bath-assisted method.[28] The detailed procedures are as follows.

A total of 100 mg of MoS_2 powder was weighed using an electronic balance (±0.1 mg accuracy) and transferred into a 100 mL glass beaker containing 50 mL of AEA. The dispersion was stirred using a magnetic stirrer at 600 rpm for 10 min to ensure preliminary uniform dispersion. The beaker was subsequently placed in an ultrasonic water bath (KQ-300DE, Kunshan Ultrasonic Instruments Co. Ltd, China) and sonicated continuously for 16 hours at a frequency of 40 kHz and power of 300 W. After sonication, the mixture was left to settle for 30 min to allow the precipitation of unexfoliated particles. The supernatant was carefully decanted and transferred to a clean glass dish. It was then dried in an electric oven at 60 °C for 12 hours to obtain MoS_2 nanosheets.

Multilayer graphene powder was treated by following a similar protocol. Specifically, 100 mg of graphene was added to 50 mL of absolute ethanol in a 100 mL beaker. After magnetic stirring at 600 rpm for 10 min, the suspension was sonicated in the same water bath ultrasonic cleaner at 40 kHz and 300 W for 30 min. After treatment, the dispersion was left undisturbed for sedimentation, and the upper suspension was collected and dried at 60 °C for 12 hours for further use.

2.3. Ultrasound assembly method

The specific steps of the ultrasonic assembly process are illustrated in Fig. 1.

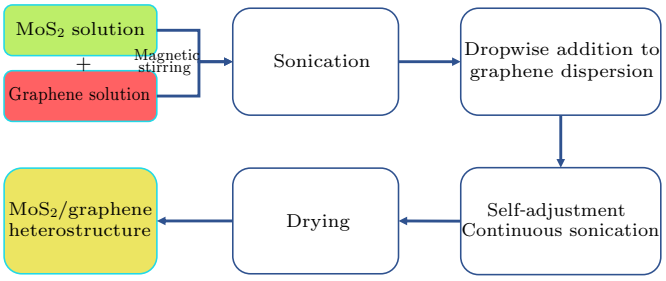


Fig. 1. Schematic illustration of the fabrication process for MoS_2/graphene heterostructures, which involves three main stages: assembly preparation, assembly and self-adjustment.

MoS_2 and graphene nanosheets were first dispersed separately. Specifically, 50 mg of MoS_2 nanosheets and 50 mg of few-layer graphene were each weighed using a precision electronic balance (±0.1 mg), and then added into separate 100 mL glass beakers containing 50 mL of AEA. The dispersions were stirred magnetically at 600 rpm for 10 min to ensure uniform mixing. Both beakers were then placed into an ultrasonic water bath cleaner and subjected to sonication at

40 kHz frequency and 180 W power for 20 min. After this initial treatment, the beaker containing the MoS_2 dispersion was removed from the ultrasonic bath, while the beaker containing the graphene dispersion remained under continuous sonication.

The MoS_2 dispersion was then slowly added dropwise into the graphene dispersion over a period of approximately 20 min using a glass dropper with a constant flow rate (about one drop every 2–3 s). Throughout the process, the graphene-containing beaker remained under ultrasonic treatment at the same frequency and power. This continuous sonication helps facilitate the uniform and stable integration of MoS_2 nanosheets onto the surface of graphene via non-covalent interactions such as vdW forces and π–π stacking.

Once the MoS_2 dispersion had been completely added, the mixed solution continued to be ultrasonicated under the same conditions for an additional 20 min to allow the heterostructure system to stabilize and undergo self-adjustment. This step enhances the uniformity and interfacial compatibility of the resulting heterostructures.

After the completion of the self-adjustment stage, the resulting MoS_2/graphene dispersion was transferred to a clean glass dish and dried in an electric oven at 60 °C for 12 hours. The final product was collected as a dry powder, representing the successfully synthesized MoS_2/graphene heterostructure. By changing the mass ratio of graphene, MoS_2/graphene heterostructures with different graphene content were prepared and named MG1, MG2 and MG3. Specifically, the graphene content in the vdW heterostructures was set to 50 wt% for MG1, 65 wt% for MG2 and 80 wt% for MG3.

2.4. Characterization

Scanning electron microscopy (SEM) was carried out on a Zeiss ΣIGMA/VP instrument operated at an accelerating voltage of 5 kV and a working distance of 6–8 mm to observe the surface morphology and microstructure of the samples. The images were captured in secondary electron mode with a resolution of approximately 3.0 nm. X-ray diffraction (XRD) analysis was performed using a SHIMADZU 6100 diffractometer with Cu $K\alpha$ radiation ($\lambda = 1.5406$ Å) to investigate the crystal structure of the samples at room temperature. The measurements were conducted over a 2θ range of 10°–80°, with a scanning rate of 4 °/min, an accelerating voltage of 40 kV and an applied current of 30 mA. Raman spectroscopy was performed using a Renishaw via confocal Raman microscope with a 514 nm laser excitation source, under ambient conditions. The laser power was set to 1%, and the spectral resolution was better than 1 cm^{-1}. X-ray photoelectron spectroscopy (XPS) was conducted on a Thermo Scientific ESCALAB Xi+ (Japan) equipped with a micro-focused monochromatic Al $K\alpha$ x-ray source ($h\nu = 1486.6$ eV). The pass energy for the survey and high-resolution scans were set to 100 eV and 20 eV, respectively. All binding energies were calibrated using the C 1s peak at 284.6 eV as a reference.

2.5. Photocatalytic experiment

The photocatalytic activity of the material is evaluated by irradiating the RhB solution with visible light. 30 mg of catalyst is added to 50 mL of 15 mg/L RhB solution. Before illumination, the reaction mixture is continuously stirred in the dark for 30 min to reach the adsorption–desorption equilibrium. Then, the mixture is illuminated with a 10 W white LED lamp (400 nm $\leq \lambda \leq$ 800 nm) in a photocatalytic reactor. Every 10 min, 5 mL of the reaction solution is collected and centrifuged to remove the photocatalyst for further measurement. The residual RhB concentration is measured using a UV–vis spectrophotometer.

3. Results and discussion

3.1. Characterization

SEM images of MoS_2 nanosheets, graphene films and assembled MoS_2/graphene heterostructures are shown in Fig. 2. From the SEM image of MoS_2 nanosheets, it can be seen that MoS_2 nanosheets like snowflakes were successfully synthesized. Carefully observing the image of the MoS_2 nanosheets given in Fig. 2(a), it is found that the size of the exfoliated MoS_2 nanosheets is mostly between 1 μm and 2 μm. The morphology of the graphene films is presented in Fig. 2(b). The graphene films in the image do not show a flat film morphology but have many wrinkles. This is because the graphene films we measured are dried graphene films rather than stretched graphene films in solution. At the same time, the overlap of different graphene films may also promote the generation of this rugged morphology. The SEM images of the assembled MoS_2/graphene vdW heterostructures with different graphene content are shown in Figs. 2(c) and 2(d). Snow-like MoS_2 nanosheets are dispersed on the curly and rugged graphene film. Due to the curling and overlapping of the graphene film after drying, it can be seen that some composited MoS_2 nanosheets are wrapped in the graphene film. At the same time, the heterostructures after drying remain stable. This is because although the dryness and the overlap of different graphene films make the surface of the graphene rugged and full of wrinkles, it still has a huge surface area compared to the snowflake-shaped MoS_2 nanosheet graphene film. This feature of graphene provides enough attachment area for the small flake-shaped MoS_2 nanosheets so that they can maintain a heterogeneous structure through vdW force bonding. Therefore, even if the composite material is dried, the MoS_2/graphene heterostructure still exists.

In addition, it can be seen from Figs. 2(c)–2(e) that as the proportion of graphene gradually increases, the probabil-

ity of heterostructure synthesis gradually decreases. When the graphene content is 50%, the ultrasonically assembled MoS_2/graphene heterostructure has the best quality and the highest material utilization rate. Since there are not enough graphene films to provide bonding points for the small MoS_2 nanosheets, as shown in Fig. 2(e), more MoS_2 nanosheets are combined with each other instead of forming a heterostructure with the graphene film. However, the MG3 sample in Fig. 2(e) has the highest graphene content. Perhaps it is precisely because the graphene content is too high that the highly extended and overlapping graphene films during assembly hinder the dispersion of MoS_2 in the solution, thereby further hindering the combination of MoS_2 and graphene. This results in the undispersed MoS_2 being able to only combine with itself, rather than with more graphene to form heterogeneous structures.

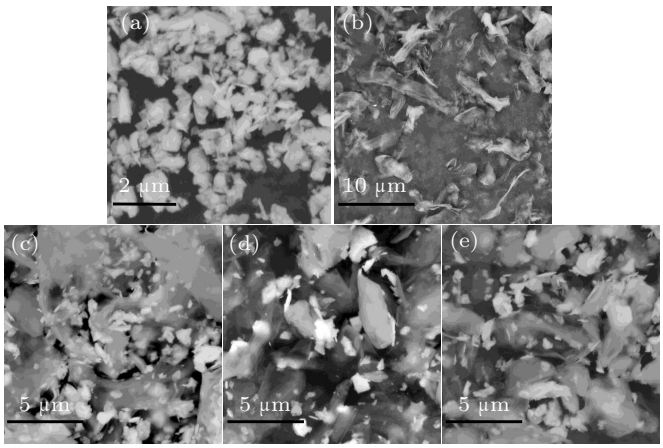


Fig. 2. SEM images of (a) MoS_2, (b) graphene, (c) MG1, (d) MG2 and (e) MG3.

The element composition and phases of MoS_2, graphene, and MoS_2/graphene heterostructures were characterized by XRD. The comparison between the XRD pattern of the measured MoS_2 and the standard card is given in Fig. S1. All the diffraction peaks of MoS_2 observed in the figure are in good agreement with the hexagonal MoS_2 of 2H phase (standard JCPDS No. 37-1429).[29,30] The strongest diffraction peak (002) of MoS_2 appears at $\theta = 14.378°$, and the two small diffraction peaks (103) and (105) appear at $\theta = 39.538°$ and $\theta = 49.787°$. The XRD pattern of graphene is basically consistent with the diffraction peaks of 3R phase graphene (standard JCPDS No. 26-1079), and is shown in Fig. S1. The strongest diffraction peak (003) of graphene appears at $\theta = 26.603°$. The XRD results of the heterostructures with different graphene mass ratios are all shown in Fig. 3. The characteristic peaks of MoS_2 and graphene can be found in all composite structures, indicating that the synthesis of MoS_2/graphene heterostructure does not change the crystal structure of MoS_2 and graphene. This also shows that the entire synthesis process of heterostructures is just a physical combination of MoS_2 and graphene using vdW force. At the same time, a new lower-intensity graphene diffraction peak appeared in the spectrum of the MoS_2/graphene composite material, which directly proved the successful synthesis of the heterostructures. Furthermore, comparing the XRD patterns of MG1, MG2 and MG3, the strongest diffraction peak of MoS_2 (002) and the characteristic peak of graphene (003) in the MG1 XRD spectrum are the strongest among the three samples. To further reveal the structure and phase of MoS_2/graphene heterostructures, Raman spectroscopy was measured as present, and is shown in Fig. 4. Compared to the spectrum of MoS_2, the E^1_{2g} and A^1_g modes of heterostructures are red-shifted, with the strongest red-shift of MG3. The phenomenon of red-shift also proves the successful combination of MoS_2 and graphene in another way.[31–33] G and 2D modes appearing at 1580 cm^{-1} and 2720 cm^{-1} are important observational features in the Raman spectrum of graphene. The appearance of the D band is due to the size reduction of the sp^2 domain in the plane during the oxidation process. Thus, the absence of the D peak in the characterized spectrum indicates that the graphene is pure without chemical bonds and edges.[34] Similar to MoS_2, the Raman spectral peaks of graphene have a red-shift in the composite structure with the highest being MG3. The Raman characteristic peaks of graphene and MoS_2 both appear in the MoS_2/graphene heterostructures and both have red-shifts. XPS results (Fig. S2) and related analysis (supporting information) reveal binding energy shifts in Mo 3d and S 2p spectra of the MoS_2/graphene heterostructures compared to pure MoS_2, indicating strong electronic interactions and confirming the formation of the heterostructure rather than simple physical mixing.[33] The presence of characteristic C 1s, Mo and S signals further supports the successful synthesis of the MoS_2/graphene heterostructures.

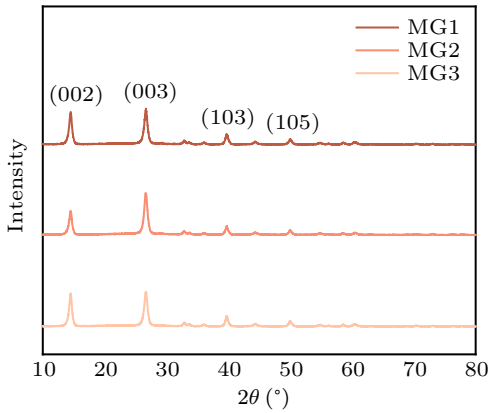


Fig. 3. XRD patterns of MoS_2/graphene heterostructures with varying graphene mass ratios, showing the characteristic peaks of both materials and confirming the successful synthesis of the heterostructures via vdW forces.

3.2. Assembly mechanism and performance analysis

Based on ultrasound theory, experimental procedures and the results of various characterizations, a potential mecha-

nism is proposed. Similar to the preparation process, the assembly mechanism is divided into three stages: dispersion, assembly and adjustment. Figure 5 presents a schematic diagram of the dispersion stage. In general liquids, ultrasound with a frequency from 20 kHz–50 MHz has wavelengths that range roughly from 10 cm to 100 μm, which are much larger than the molecular scale. Therefore, the chemical and physical effects of ultrasound in the material synthesis process do not arise from the direct interaction between the material and ultrasound, but from the physical phenomenon of acoustic cavitation.[35,36] This physical phenomenon involves three processes: formation, growth and implosive collapse of bubbles.[37] When sound waves of sufficient amplitude are transmitted into the liquid, micro air-core cavitation bubbles are generated. Bubbles of critical size (typically around 10 μm) strongly couple with the acoustic field, undergo rapid inertial overgrowth during expansion, and ultimately collapse, releasing a significant amount of energy. This release of internal energy facilitates the uniform dispersion of MoS_2 nanosheets and graphene films in the solution. Moreover, SEM observations revealed that a higher mass ratio of graphene in the sample hindered the dispersion of MoS_2 due to the extensive size and surface area of graphene in the solution, leading to the aggregation of MoS_2 nanosheets, which indicates the presence of a dispersion stage. These findings suggest that the dispersion stage is necessary to overcome the agglomeration of nanosheets.

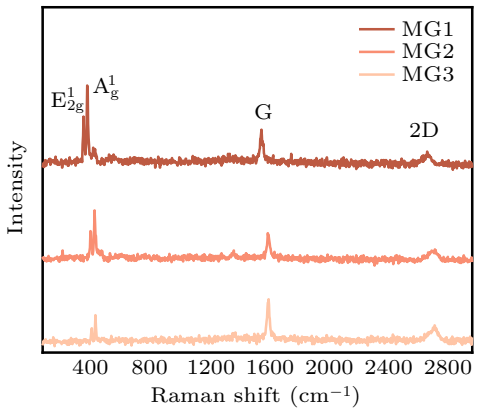


Fig. 4. Raman spectra of MoS_2/graphene heterostructures, showing red-shifted E^1_{2g} and A^1_g modes of MoS_2 and characteristic peaks of graphene (G and 2D bands), confirming the successful integration of MoS_2 and graphene without chemical bonding.

As shown in the inset image zoomed in from Fig. 5, while the dispersion process is occurring, assembly is simultaneously taking place. According to the Raman spectrum and XPS characterization results, there is a force interaction between MoS_2 and graphene, rather than a pure physical mixing, indicating the presence of an assembly stage that assembles the two 2D materials into vdW heterostructures. In this stage, numerous dispersed MoS_2 nanosheets and the extended graphene in the solution are attracted to each other through vdW forces, forming a heterostructure. Meanwhile, the energy generated by the acoustic cavitation process is sufficient to break the weak vdW bond between MoS_2 and graphene.[36,38–47] As a result, the dispersed MoS_2 nanosheets are continuously combined with the graphene surface during the assembly process. However, the energy released by bubble collapse, the shock waves generated by the rebound of the collapsed bubble, the jets produced by the interaction between the bubble and the material, and the intensified thermal motion after the liquid molecules absorb the energy all cause constant interruptions in this combination, leading to a more uniform dispersion of the MoS_2 nanosheets.[36,44,48–50]

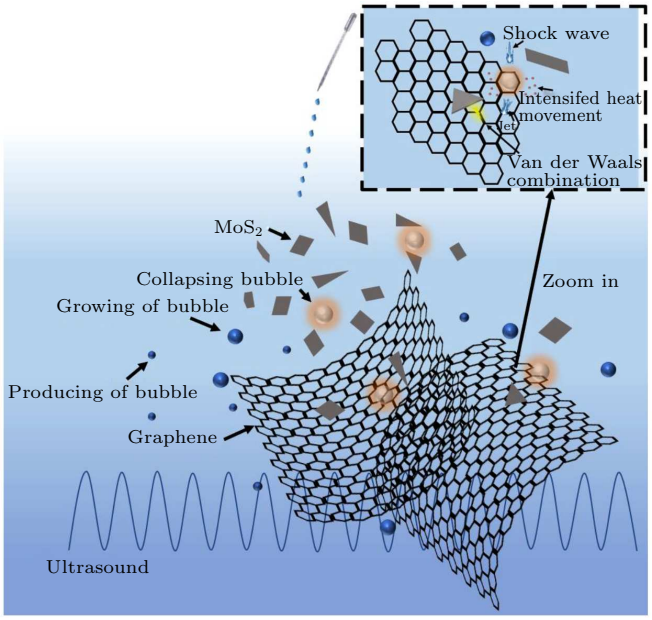


Fig. 5. Schematic illustration of the ultrasound-assisted assembly mechanism of MoS_2/graphene heterostructures. Simultaneous dispersion and assembly driven by vdW forces and acoustic cavitation effects.

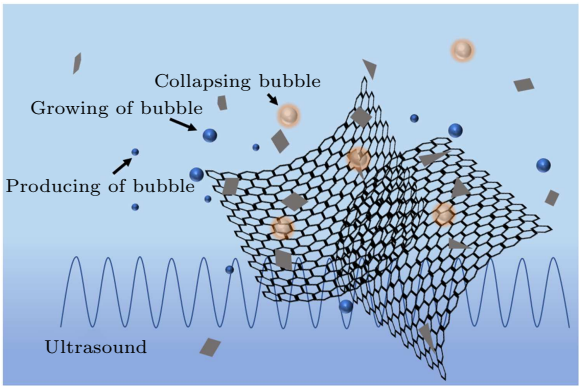


Fig. 6. Schematic illustration of the ultrasound-assisted assembly mechanism of MoS_2/graphene heterostructures. Adjustment phase involving refinement and optimization of heterostructure integration.

As depicted in the adjustment phase of Fig. 6, the assembly stage persists with a critical distinction from prior stages; no additional MoS_2 nanosheets are introduced into the system at this juncture. By this point, both the dispersion equilibrium of MoS_2 nanosheets and their heterogeneous integration

with graphene films have been substantially achieved, marking the transition to refinement rather than further material incorporation. Sustained ultrasonic treatment primarily serves to refine the morphology and enhance dispersion of MoS_2 sheets, while simultaneously facilitating their optimal integration with graphene films to engineer a robust vdW heterogeneous nanocomposite interface.

To demonstrate the practical application potential of the synthesized MoS_2/graphene vdW heterostructure, a photocatalytic experiment was conducted to evaluate its photocatalytic performance. Based on the SEM, XRD and Raman spectroscopy results, the MG1 sample was selected as the photocatalyst and tested under illumination from a 10 W white LED lamp. As shown in Fig. 7, the MG1 sample achieved a RhB degradation rate of up to 91.3%. A performance comparison with MoS_2/graphene heterostructures prepared by other methods is presented in Table 2, highlighting the superior photocatalytic efficiency of the material synthesized via the ultrasonic assembly approach.[51–54]

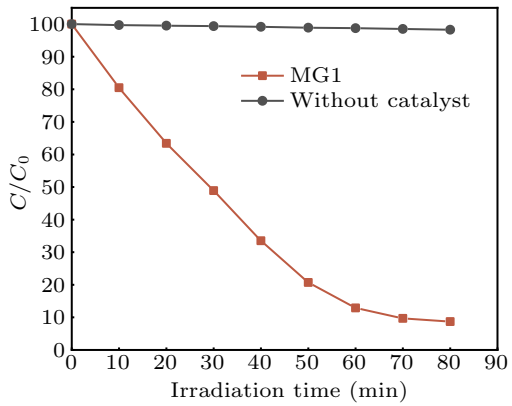


Fig. 7. Photocatalytic degradation efficiency of MG1 prepared by the ultrasonic assembly method.

Table 2. Comparison of photocatalytic performance of MoS_2/graphene-based photocatalysts synthesized by different methods for RhB degradation.

Photocatalyst	Catalyst mass (mg)	Organic concentration ($mg \cdot L^{-1}$)	Degradation date	Reaction time (min)	Light source	Preparation method	Ref.
MoS_2/rGO heterostructures	100	20	80%	240	Compact lamp (60 w–220 V)	Ultrasonic treatment and hydrothermal method	[51]
MoS_2/reduced graphene oxide composites	10	10	71.74%	180	1 kW Xe lamp	Hydrothermal method	[52]
Ternary GO/g-C_3N_4/MoS_2 flower-like heterojunctions	20	20	77.20%	60	300 W Xe lamp	Ultrasonic treatment and hydrothermal method	[53]
$ZnSnO_3$/rGO/MoS_2 nanocomposite	10	100	78%	100	500 W halogen lamp	Solid-state reaction method	[54]
MoS_2/graphene vdW heterostructures	30	15	91.30%	80	10 W white LED lamp	Ultrasound assembly	This study

4. Conclusion

In summary, MoS_2/graphene vdW heterostructures were successfully fabricated using a convenient ultrasound assembly method, demonstrating the potential of the ultrasonic path for synthesizing 2D heterogeneous structures. The ultrasonic assembly process, based on the ultrasonic path, involves three main stages: assembly preparation, assembly and self-adjustment. The morphology of MoS_2 nanosheets, graphene films and composite materials was observed through SEM. The successful fabrication of heterostructures was confirmed through XRD, Raman and XPS analysis. A red-shift in the Raman spectrum of the composite structures and a decrease in binding energy in the Mo 3d and S 2p XPS spectra indicate successful heterostructure formation. These results provide sufficient evidence that the ultrasonic path is a feasible and effective approach for manufacturing heterostructures. The proposed mechanism for fabrication involves three stages: dispersion, assembly and adjustment. Acoustic cavitation, a key element of ultrasonic sonochemistry, plays a major role in these stages.

However, while the ultrasonic assembly method shows significant promise, some limitations remain. The scalability of the method for large-scale production, the stability of the heterostructures over extended periods, and the control over uniformity at larger scales need further investigation. Moreover, the influence of ultrasonic frequency and power on the final properties of the heterostructures warrants deeper exploration.

Looking ahead, future research will focus on optimizing the ultrasonic assembly process for industrial applications, improving the reproducibility and scalability of the method, and exploring other 2D material combinations for heterostructure fabrication. In addition, further studies on the long-term stability and potential environmental impact of these materials are crucial for their practical use in various applications such as sensors, energy storage and electronic devices.

Acknowledgements

This study was supported by the China Inner Mongolia Autonomous Region Directly-Undergraduate Universities Basic Research Business Fund Project: ‘Environmental Protection Equipment R&D’ Shared Technology and Skills Innovation Platform Construction (Grant No. NJDYWF2301).

References

[1] Novoselov K S, Mishchenko A, Carvalho A and Castro Neto A H 2016 *Science* **353** aac9439
[2] Wang W, Cheng B, Luo G Q, Yu J Ga and Cao S W 2024 *Materials Today* **81** 137

[3] Goel N, Utkarsha, Kushwaha A, Kwoka M, Kumar R and Kumar M 2024 *Journal of Materials Chemistry A* **12** 5642
[4] Liu W J, Wu Y F, Bao X Z D, Sun L, Xie Y E and Chen Y P 2025 *Advanced Functional Materials* **04** 2421525
[5] Carvalho A, Wang M, Zhu X, Rodin A S, Su H B and Castro Neto H C 2016 *Nature Reviews Materials* **1** 16061
[6] Chen H L, Wen X W, Zhang J, Wu T M, Gong Y J, Zhang X, Yuan J T, Yi C Y, Lou J, Ajayan PM, Zhuang W, Zhang G Y and Zheng J R 2016 *Nat. Commun.* **7** 12512
[7] Tang S W, Ai P, Bai S L, Wan D, Li X D, Guo W R, Zhen T and Wang H 2024 *Materials Today Physics* **43** 101398
[8] Guo H W, Hu Z, Liu Z B and Tian J G 2021 *Advanced Functional Materials* **31** 2007810
[9] Rafi R, Rahulan K M, Flower N A L, Abith M, Chidambaram S G T and Rajendran A S 2024 *ACS Applied Nano Materials* **7** 11097
[10] de Sousa B P, Estrada A C, Trindade T and Fateixa S 2025 *Applied Surface Science* **689** 162492
[11] Jacobo J R, Olea-Mejía O F, Martínez-Hernández A L and Carlos V S 2024 *FlatChem* **45** 100654
[12] Gao H G, Shi R, Shao Y T, Liu Y N, Zhu Y F, Zhang J G, Hu X H, Li L Q and Ba Z X 2022 *J. Alloys Compd.* **895** 162635
[13] Guan X S, Zhang X C, Zhang C M, Li R, Liu J X, Wang Y F, Wang Y W, Fan C M and Li Z 2023 *Journal of Colloid and Interface Science* **644** 426
[14] Mei J, Liao T and Sun Z Q 2022 *Energy & Environmental Materials* **5** 115
[15] Xiang T, Chen F X, Li X L, Wang X D, Yan Y L and Wang L S 2023 *Chin. Phys. B* **32** 117301
[16] Xie N H, Chen W Z, Ning Y and Zeng X J 2024 *Materials Today Nano* **28** 100529
[17] Akimov A V, Neukirch A J and Prezhdo O V 2013 *Chem. Rev.* **113** 4496
[18] Kim S, Lee C, Lim Y S and Shim J H 2021 *ACS Omega* **6** 278
[19] Rathi S, Lee I, Lim D, Wang J W, Ochiai Y, Aoki N, Watanabe K, Taniguchi T, Lee GH, Yu Y J, Kim P and Kim G H 2015 *Nano Lett.* **15** 5017
[20] Wu F F, Li L, Xu Q L, Liu L, Yuan Y L, Zhao J J, Huang Z H, Zan X Z, Watanabe K, Taniguchi T, Shi D X, Xian L D, Yang W, Du L J and Zhang G Y 2023 *Chin. Phys. Lett.* **40** 047303
[21] Sheng Q L, Qiao X J, Zhou M, Yue T L and Zheng J B 2019 *Handbook of Graphene Set: Biosensors and Advanced Sensors* (New York: Wiley) 535
[22] Swain G, Sultana S and Parida K 2021 *Nanoscale* **13** 9908
[23] Cao Q, Dai J J, Hao Z T, Paulus B, Eigler S and Chen X 2024 *Angewandte Chemie International Edition* **63** 202415922
[24] Zhang X W, Biekert N, Choi S, Naylor C H, De-Eknamkul C, Huang W Z, Zhang X J, Zheng X R, Wang D K, Johnson A T C and Cubukcu E 2018 *Nano Lett.* **18** 957
[25] Dastidar M G, Basu N, Kao I H, Katoch J, Nayak P K, Singh S and Bhallamudi V P 2024 *Nanoscale* **16** 19413
[26] Bhat S, Banday J and Wahid M 2023 *Energy Fuels* **37** 6012
[27] Song S, Lyu J, Qin L, Wang Z, Gong J and Yang S Y 2024 *Phys. Rev. B* **110** 125407
[28] Gao M Y, Zhang Z Y, Zhang W, Yao X, Cao Z, Cao Q Z, Zhu H Y and Zhao W 2021 *FlatChem* **30** 100312
[29] Hou M Z, Qiu Y T, Yan G F S, Wang J M, Zhan D, Liu X, Gao J C and Lai L F 2019 *Nano Energy* **62** 299
[30] Zhang J, Huang G Z, Zeng J H, Jiang X D, Shi Y X, Lin S J, Chen X, Wang H B, Kong Z, Xi J H and Ji Z G 2019 *J. Alloys Compd.* **775** 726
[31] Kong D S, Wang H T, Cha J J, Pasta M, Koski K J, Yao J and Cui Y 2013 *Nano Lett.* **13** 1341
[32] Pandey A, Mukherjee A, Chakrabarty S, Chanda D and Basu S 2019 *ACS Applied Materials & Interfaces* **11** 42094
[33] Liu Y, Zhou Y, Zhang H, Ran F R, Zhao W H, Wang L, Pei C J, Zhang J D, Huang X and Li H 2019 *Frontiers of Physics* **14** 13607
[34] Nanda S S, Kim M J, Yeom K S, An S S A, Ju H and Yi D K 2016 *TrAC Trends in Analytical Chemistry* **80** 125
[35] Suslick K S 1990 *Science* **247** 1439
[36] Brenner C R 1995 *Cavitation and Bubble Dynamics* (Oxford: Oxford University Press)
[37] Xu H X, Zeiger B W and Suslick K S 2013 *Chem. Soc. Rev.* **42** 2555
[38] Leighton T G 1994 *The Acoustic Bubble* (London: Academic Press)
[39] Wang P Q, Jia C C, Huang Y and Duan X F 2021 *Matter* **4** 552
[40] Flint E B and Suslick K S 1991 *Science* **253** 1397
[41] Suslick K S, Eddingsaas N C, Flannigan D J, Hopkins S D and Xu H X 2018 *Accounts of Chemical Research* **51** 2169
[42] Flannigan D J and Suslick K S 2005 *Nature* **434** 52
[43] Didenko Y T and Suslick K S 2002 *Nature* **418** 394
[44] Didenko Y T, McNamara W B and Suslick K S 2000 *Nature* **407** 877
[45] McNamara W B, Didenko Y T and Suslick K S 2000 *J. Am. Chem. Soc.* **122** 8563
[46] Lee J H, Avsar A, Jung J, Tan J Y, Watanabe K, Taniguchi T, Natarajan S, Eda G, Adam S, Neto A H C and Özyilmaz B 2015 *Nano Lett.* **15** 319
[47] Tanabe T, Tang C, Sato Y and Oyama Y 2018 *J. Appl. Phys.* **123** 245107
[48] Lauterborn W and Kurz T 2010 *Reports on Progress in Physics* **73** 106501
[49] Vogel A and Lauterborn W 1988 *Appl. Opt.* **27** 1869
[50] Vogel A, Hentschel W, Holzfuss J and Lauterborn W 1986 *Klinische Monatsblatter Fur Augenheilkunde* **189** 308
[51] Phan T T T, Nguyen T T H, Huu H T, Truong T T, Nguyen L T, Nguyen V T, Tran V A, Nguyen T L, Nguyen H L and Vo V 2021 *Journal of Nanomaterials* **2021** 9941202
[52] Zhang L, Sun L, Liu S, Huang Y, Xu K and Ma F 2016 *RSC Advanced* **65** 60318
[53] Wu M, Li L, Xue Y, Xu G, Tang L, Liu N and Huang W 2018 *Applied Catalysis B: Environmental* **228** 103
[54] Venkatesh G, Elavarasan N, Srinivasan M, Palanisamy G, Macadangdang R R Jr., Vignesh S, Ramasamy P, Ali H E, Shkir M and Ahmad Z 2022 *International Journal of Hydrogen Energy* **47** 11863